Rare Met. (2016) 35(2):140–148
DOI 10.1007/s12598-015-0675-2

RARE METALS
www.editorialmanager.com/rmet

Fabrication and characterization of anodic oxide nanotubes on TiNb alloys

Ming Jin, Xin Lu, Yi Qiao, Lu-Ning Wang*, Alex A. Volinsky

Received: 26 August 2015 / Revised: 28 September 2015 / Accepted: 25 November 2015 / Published online: 2 January 2016

Abstract Titanium and its alloys have been extensively used as implant materials owing to their high specific strength, good biocompatibility and excellent corrosion resistance. Oxide nanotubular array layer can be formed on Ti alloy surface by electrochemical anodization treatment. In this work, the morphology of nanotubes formed on Ti–Nb alloys (Nb content of 5 wt%, 10 wt%, 20 wt%, 30 wt% and 40 wt%) was investigated using an electrolyte containing ethylene glycol and NH_4F. Oxide layers consisting of highly ordered nanotubes with a range of diameters (approximately 40–55 nm for the inner diameter and 100–120 nm for the outer diameter) and lengths (approximately 10–20 μm) can be formed on alloys in the Ti–*x*Nb system, independent on the Nb content. The nanotubes formed on the Ti–Nb alloy surface were transformed from the anatase to rutile structure of titanium oxide. The oxide nanotubular surface is highly hydrophilic compared with the intact TiNb foil. The surface wettability varies with the nanotube diameter. As the nanotube diameter increases while the nanotube layer thickness remains constant, the capillary wetting of the nanotube surface decreases and the surface becomes less hydrophilic. Annealing changes the nanotubular surface wettability further and establishes less hydrophilic surface conditions due to the removal of hydroxyl groups and residue fluoride-containing species. It is believed that the surface wettability is changed due to the decreasing content of hydroxyl groups in ambient atmosphere. This work can provide guidelines for improving structural and environmental conditions responsible for changing surface wettability of TiNb surfaces for biomedical applications.

Keywords Ti–Nb alloy; Anodization; Nanotubes; Wettability; Implants

1 Introduction

Titanium and its alloys, such as Ti–6Al–4V and Ti–6Al–7Nb, are widely utilized as implant materials owing to the combination of excellent strength, corrosion resistance, outstanding biocompatibility and hemocompatibility. Biocompatibility of titanium and its alloys is due to the formation of a thin naturally formed oxide layer (2–3 nm) on the metal surface, which retards the dissolution of ions and other reactions with surrounding tissues [1]. However, mismatch of elastic modulus between the implants and bones could cause prostheses loosening [2]. Moreover, Al has been considered potentially toxic and carcinogenic after a long-term service span [3]. Sustainable efforts thus have been undertaken to develop novel nontoxic elements containing titanium alloys with lower elastic modulus. Compared with cp-Ti and Ti–6Al–4V, β-type titanium alloys with relatively low elastic modulus are desirable because they can minimize the bone resorption effects from stress shielding during service [4, 5]. Many efforts have been made to fabricate β-type titanium alloys as novel implant candidates [6, 7]. And it is well known that the stability of β phase and β-transus temperature in titanium

M. Jin, X. Lu, L.-N. Wang*
School of Materials Science and Engineering, University of Science and Technology Beijing, Beijing 100083, China
e-mail: luning.wang@ustb.edu.cn

Y. Qiao
State Key Laboratory for Advanced Metals and Materials, University of Science and Technology Beijing, Beijing 100083, China

A. A. Volinsky
Department of Mechanical Engineering, University of South Florida, Tampa, FL 33620, USA

alloys are significantly influenced by the element ratio. Niobium with excellent mechanical, chemical and biocompatible properties can enable applications of corrosion-resistant structural materials and biomedical implants, acting as a β-stabilizer. More recently, Ti–Nb alloys with 40 wt% Nb content have been reported as novel materials for biomedical applications [8].

Metallic implants typically have a thin layer of fibrous tissue at the bone–implant interface. The existence of this layer becomes a major challenge to decelerate the process of osseointegration and to extend the implant fixation time. Fast fixation is crucial for the success rate of implantation and can reduce the micromotion of implants and minimize the formation of fibrous tissue, leading to early physiological loading and preventing the bone from disuse atrophy. In addition, fast fixation of implants reduces the hospitalization time and cost and improves patient quality of life. As a result, many attempts have been made to improve the interaction between bone and implants. One of the most actively pursued areas is the development of novel surfaces by surface modification to improve the implants' surface properties and facilitate faster osseointegration and healing processes.

Electrochemical anodization is a versatile technique, which has already been used to grow thick and uniform oxide layers on metals for decades and has shown significant advantages to enhance metallic implants' biocompatibility [9]. A protective oxide layer with controlled and desired thickness is spontaneously formed by using metal as the anode in an electrochemical cell. The structure of the oxide layer can be tailored by tuning the type of electrolyte, applied current density, electrolyte concentration and temperature, and agitation speed along with the cathode-to-anode and surface-to-area ratios [10–12]. Following the very first paper published by Assefpour-Dezfuly et al. [13] in 1984, the formation of anodic TiO_2 nanotubular arrays on Ti has surpassed porous alumina in a number of papers. TiO_2 nanotubes formed by anodizing are open at the top and closed at the bottom, and their sizes can be changed by controlling the concentration and type of electrolyte, time and voltage. Because of the unique biocompatibility of TiO_2 nanotubular arrays, several excellent reviews have been published to demonstrate the fabrication of TiO_2 nanotubular arrays and their applications in implants [14]. Park et al. [15] demonstrated that by varying the anodic potential and the concentration of fluoride species, the cell viability can be tailored on TiO_2 nanotubular arrays with optimal geometry. Wilmowsky et al. [16] studied the effects of TiO_2 nanotube structured surface on bone formation in vivo compared with an untreated standard titanium surface in pigs. Sorkin et al. [17] investigated the use of two different morphologies of titania nanotube arrays as interfaces to advance the longevity and effectiveness of neural prostheses.

Apart from pure Ti, there has been much interest in fabricating nanotubes on the surface of binary titanium alloys, such as Ti–Zr, Ti–Ta, Ti–Al, Ti–Mo and Ti–W [10, 18–20]. The diameter, shape and distribution of these metal oxide nanotubes, formed on the surfaces of these alloys, were related to the alloy element concentration. However, only few studies focused on fabrication and bioactivity of oxide nanotubes on Ti–Nb alloys. The influence of Nb content and anodization parameters on the formation of oxide nanotubular arrays has not been fully investigated. Additionally, wettability is an essential characteristic of surfaces for biomedical applications. Thus, the corresponding wettability characteristics along with the variation in wettability of nanotubular arrays on TiNb alloy with respect to diverse geometries were rarely reported or not comprehensively understood. In the present study, nanotubular arrays on TiNb alloys with different Nb contents were fabricated and tested under various operating conditions to evaluate the effect of Nb on the formation of nanotubular arrays. The wettability and surface topography of the as-formed nanotubes were also investigated. Meanwhile, the transition of wettability during the annealing treatment was studied using contact angle measurement, Fourier transform infrared (FTIR) spectroscopy and X-ray photoelectron spectroscopy (XPS).

2 Experimental

Ti–Nb alloy (Nb content = 5 wt%–40 wt%) foils with 10 mm × 15 mm × 1 mm size were cut from Ti–Nb alloy ingot. The specimens were polished mechanically up to 2000 grit using emery paper and then ultrasonically cleaned with acetone, ethanol and deionized water, respectively, and finally dried in air. Each foil was then etched in a solution containing $HF/HNO_3/H_2O$ (1:4:2 volume ratio) for 1 s [21]. Anodization of the alloys was performed in a two-electrode configuration, where Ti–Nb alloy plates were used as the working electrode and a 1.5 cm × 1.5 cm platinum foil was used as the counter electrode under constant potential at room temperature. A direct current (DC) power supply (Maynuo M8813) was used as the voltage source to drive the anodization. The electrochemical experiments were performed in the electrolyte consisted of ethylene glycol, 0.068 $mol \cdot L^{-1}$ NH_4F and 2 vol% H_2O with a two-step anodization method. The specimens were first anodized for 1 h and then washed during sonication to remove the as-formed anodic layer, followed by an identical anodization for 0.5 h. After the electrochemical treatment, the samples were rinsed with deionized water and then dried in a compressed air stream. Some of the specimens were annealed at 450 and 850 °C for 1 h with the heating rate of 5 $°C \cdot min^{-1}$ to convert the amorphous phase into the crystalline structure.

For morphological characterization of the samples, field emission scanning electron microscopy (SEM, ZEISS Auriga) was used. In order to observe the tubular diameter and the wall thickness, transmission electron microscopy (TEM, JEM-2010) was utilized. X-ray diffractometer (XRD, STOFDARMSTADT, STOE/2, Cu Kα radiation) was used to examine the crystalline structure of the samples. The scanning range was $2\theta = 10°–90°$, and the scanning rate was 4 (°)·min^{-1}. Surface roughness of the pure Ti and oxide nanotubular arrays on Ti20Nb anodized at 20 V (Ti20Nb-20) and 60 V (Ti20Nb-60) was measured by a laser scanning confocal microscope (LSCM, OLYMPUS, LEXT). Contact angle measurements of deionized water and glycerol were taken in equilibrium conditions with the contact angle setup from the Orbisphere Laboratories, Switzerland (water droplet volume of 14 μl) with a goniometer (Shanghai Zhongchen Digital Technique Apparatus Co., Ltd., JC200C4). Optical images were acquired by a charge-coupled device (CCD) camera interfaced with a computer. Fourier transform infrared spectra (FTIR, Bruker) were employed to analyze the functional groups present on the sample surfaces, and an X-ray photoelectron spectroscopy (XPS, Kratos AXIS Ultra DLD) was used to detect the elements on the surfaces.

3 Results and discussion

3.1 Fabrication of anodic nanotubular arrays on Ti–*x*Nb alloys

The morphologies of the oxide nanotubular arrays and their cross-sectional structures on Ti–Nb alloy with different Nb contents anodized at 60 V for 0.5 h are shown in Fig. 1 for Ti–*x*Nb alloys. It is apparent that these nanotubes are open at the top and closed at the bottom. The cross-sectional view was taken from mechanically scratched samples, where some pieces flake off. The geometrical data of the inner and outer diameters of the nanotubular arrays formed on the Ti–*x*Nb alloys are portrayed in Fig. 2a. For instance, the inner and outer diameters of the Ti5Nb are 42 and 118 μm, respectively. Under the present anodization conditions for nanotubular array formation, highly ordered self-organized oxide nanotubular arrays are formed with the inner diameter ranging from 40 to 50 nm and the outer diameter ranging from 120 to 140 nm on Ti–*x*Nb alloys. Although there is a fluctuation in the diameter values, it is evident that the amount of Nb in the binary Ti–Nb alloys has little influence on the as-formed nanotubular arrays. Similar to the tendency shown in Fig. 2a, Fig. 2b illustrates the variation in the wall thickness and nanotubular array thickness on Ti–*x*Nb alloys. It can be observed that the wall

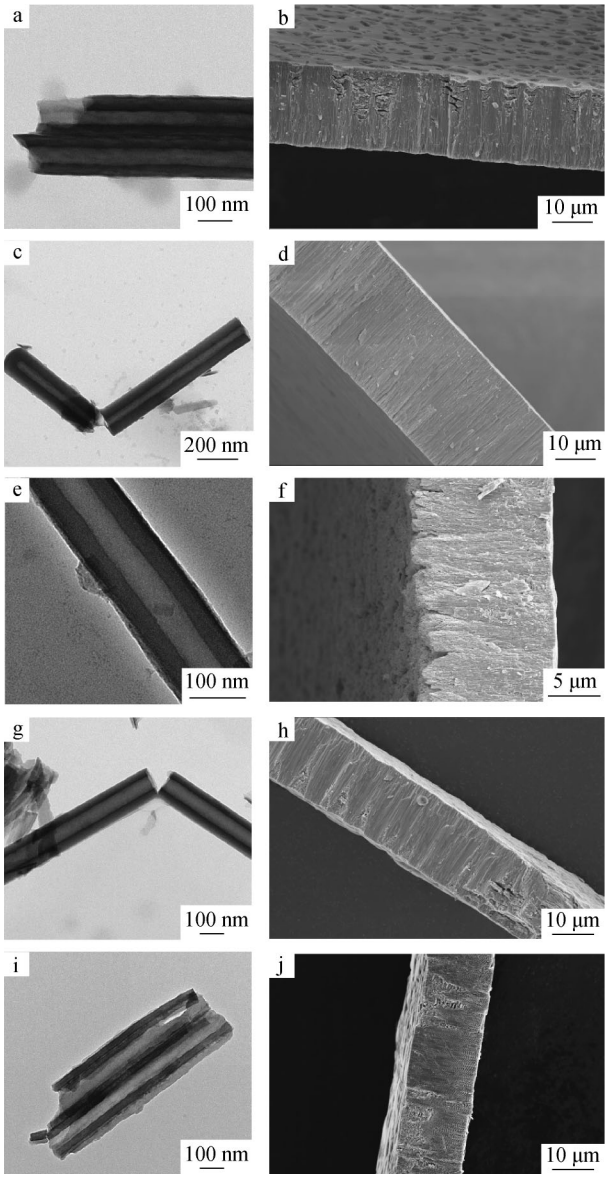

Fig. 1 TEM images of morphology (**a**, **c**, **e**, **g**, **i**) and SEM images of cross-sectional view (**b**, **d**, **f**, **h**, **j**) of nanotubular arrays formed on **a**, **b** Ti5Nb, **c**, **d** Ti10Nb, **e**, **f** Ti20Nb, **g**, **h** Ti30Nb and **i**, **j** Ti40Nb oxide nanotubes anodized at 60 V

thickness ranges from 40 to 45 nm, while the layer thickness ranges from 10 to 20 μm for all alloys. Nanotube array geometry is independent of the Nb content under present condition.

The nanotubular array formation in fluoride-containing electrolyte is a result of three simultaneous processes: (1) electric field-assisted oxidation of titanium and niobium to form metallic oxide; (2) electric field-assisted dissolution of titanium ions in electrolyte; and (3) chemical dissolution of metals and metallic oxide by fluoride ions etching. The formation of the oxide nanotubular arrays is most likely enhanced by the stimulated electric field, as observed in

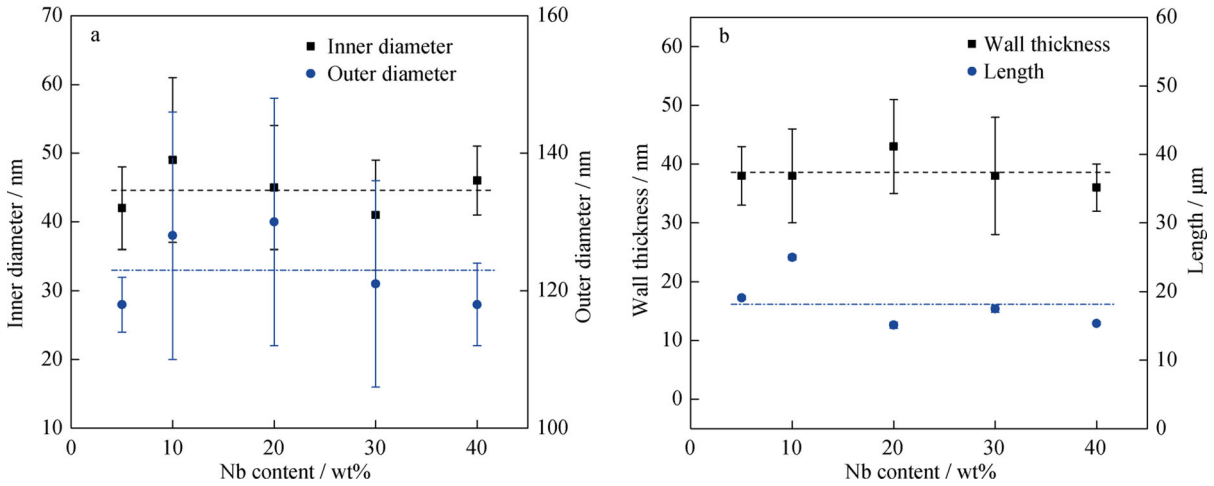

Fig. 2 Inner and outer diameters of nanotubular arrays **a** and wall thickness and nanotube length **b** formed on Ti–Nb alloys anodized at 60 V with respect to Nb content

Al_2O_3 and TiO_2 [22]. Inside these tubes, there are two interfaces: oxide/metal and oxide/anodizing solution. The electric field-enhanced oxidation occurs at the oxide/metal interface near the nanotube bottom when the oxygen-containing anions, such as O^{2-} and OH^-, are transported from the solution to the oxide layer along the nanotube growth direction. At the same time, metal ions migrate from the metal to the solution/oxide interface and dissolve into the solution. The electric field and concentration field can enhance the migration and diffusion of metal ions. The metal dissolution rate at the bottom is far greater than that at the wall, resulting in perpendicular growth of the channel with high aspect ratio. It is anticipated that some similar processes are operative in the metallic nanotubular arrays shown in Fig. 1. On the other hand, oxide dissolution reactions depend on the oxide film structure, such as TiO_2 and Nb_2O_5 for Ti–*x*Nb alloys. Since the diffusion coefficient of Ti is greater than that of Nb, the migration rate of Ti is greater than that of Nb to form the oxide. It can be deduced that the formation of nanotubular arrays on the Ti–*x*Nb alloys is independent on the content of Nb in the present alloys. Energy-dispersive X-ray spectroscopy (EDX) was applied to check the Ti/Nb ratio along the tubes, finding that for Ti5Nb (raw Ti/Nb weight ratio is 19:1), a higher Ti/Nb weight ratio of 2.1:1.0 (not shown here) in the tube is obtained, which indirectly supports the above-mentioned hypothesis.

To study parameter dependence of the nanotubular arrays on Ti–*x*Nb, Ti20Nb was chosen as an example to carry out the following characterization. Figure 3 shows SEM images of nanotubes on the Ti20Nb alloy. From the top view of these images (Fig. 3a–c), nanotube arrays with uniform diameter form in the three samples stimulated by different applied voltages. This may due to the weaker acidity/dissolution strength of the electrolytes used. A similar phenomenon was also reported by others [23]. Comparison study of these three samples demonstrates that the driving voltage has a strong influence on the morphology of the Ti20Nb nanotubes. The outer diameter of the nanotubes (calculated from 100 nanotubes) increases from 46 nm at 20 V to 130 nm at 60 V. The thickness of the array layer can also be tuned by varying the driving voltage, as shown in the inset of Fig. 3a–c. The thickness of the nanotube arrays is approximately 3 μm at 20 V and monotonically increases to 14 μm at 60 V. This is likely due to the enhancement of anodic current for the nanotube formation, provided that the applied potential would lead to an increase in the nanotubular diameter and the layer thickness simultaneously [14, 24].

Different pore sizes of the nanotube array would result in different surface roughness. Mean roughness (R_a) and root-mean-square (RMS) roughness (R_q) were utilized to evaluate the 3D surface morphology. These parameters represent an overall description of the surface texture, allowing differentiating peaks, valleys and the spacing of surface texture [25]. LSCM images of the samples are shown in Fig. 4. In the present study, the roughness amplitude parameters R_a and R_q decrease with the applied potential increasing from 20 to 60 V (Table 1). For instance, the R_a value for Ti20Nb-20 is 0.31 μm, while the R_a value for Ti20Nb-60 is 0.24 μm. Both surfaces are rougher than that of the neat alloy.

XRD patterns of Ti20Nb nanotubes before and after annealing at 450 and 850 °C are shown in Fig. 5. For the initially formed nanotubes on Ti20Nb alloy, there are no TiO_2 or Nb_2O_5 reflections, indicating their amorphous structure. For the as-formed nanotubes, only some peaks are observed, indicating Ti metal phases. After annealing at 450 °C, diffraction peak intensity at approximately 25°

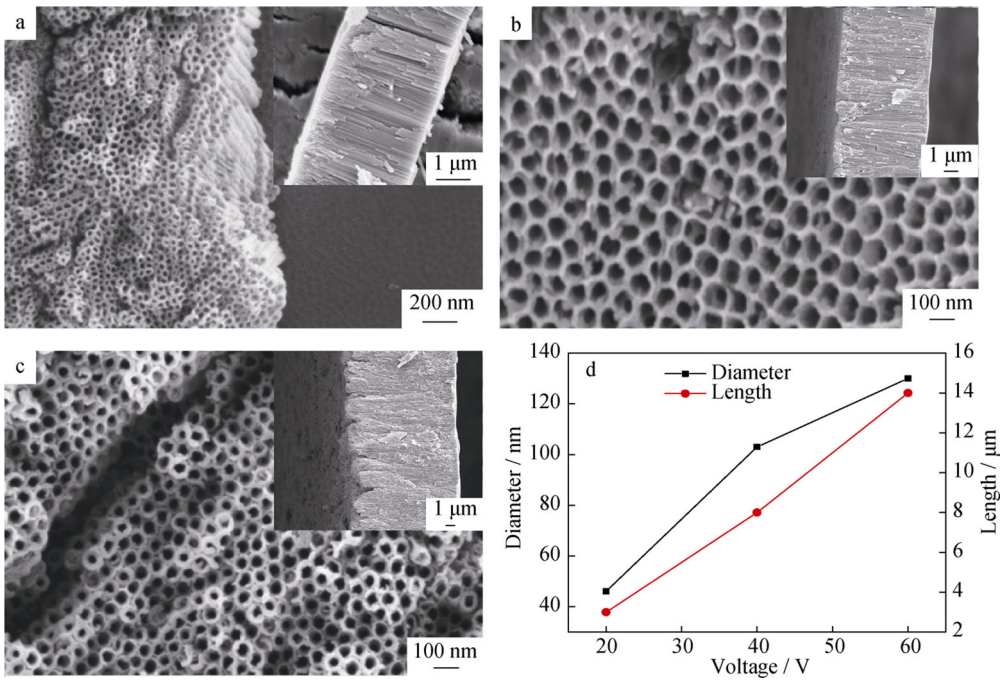

Fig. 3 Surface morphology and cross-sectional view (inset) of Ti20Nb anodized at different voltages: **a** 20 V, **b** 40 V and **c** 60 V with oxidation time of 1.0 and 0.5 h; **d** relationship of nanotubular diameter and thickness with respect to anodic voltage

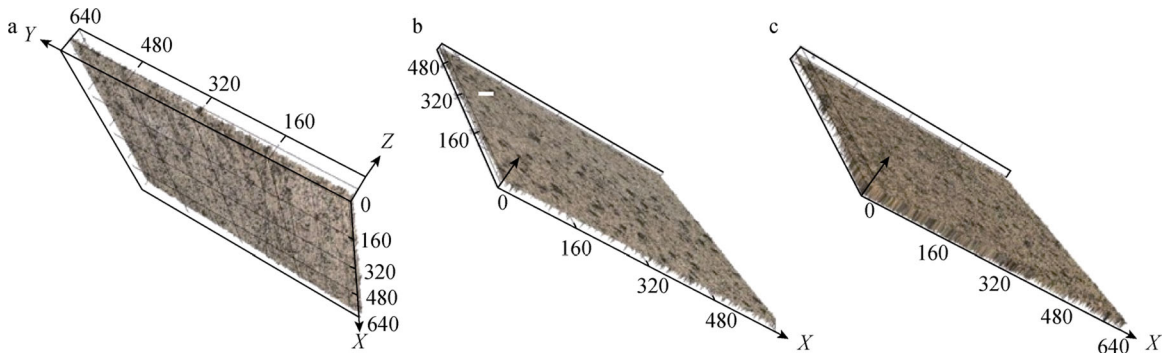

Fig. 4 LSCM images of **a** pure alloy and Ti20Nb alloy oxide nanotubes anodized at **b** 20 V and **c** 60 V

begins to appear which is the strongest diffraction reflection of anatase. After annealing at 850 °C, rutile peaks appear, but anatase remains the major TiO_2 phase. However, in the two samples with different annealing temperatures, no niobium diffraction peaks are observed. The absence of Nb reflections in the as-formed and annealed nanotubes is attributed to the undetectable amount of Nb in the nanotubes after anodization and even after annealing because of the very low diffusion coefficient of Nb compared to that of Ti. This result is consistent with the morphology of nanotubular arrays, where no significant difference is observed on all Ti–*x*Nb alloys with different Nb contents.

Table 1 Roughness of pure alloy, Ti20Nb alloy oxide nanotube anodized at 20 and 60 V

Samples	R_a/μm	R_q/μm
Pure alloy	0.12	0.159
Ti20Nb-20	0.31	0.390
Ti20Nb-60	0.24	0.313

3.2 Wettability of anodic nanotubular arrays

Hydrophobicity and hydrophilicity reflect wetting properties of a surface. Accepted definitions generally consider water contact angle as follows: (1) superhydrophobic with static water contact angle >150°, (2) hydrophobic with water contact angle between 90° and 150°, (3) hydrophilic with water contact angle between 10° and 90° and (4) superhydrophilic with water contact angle <10°.

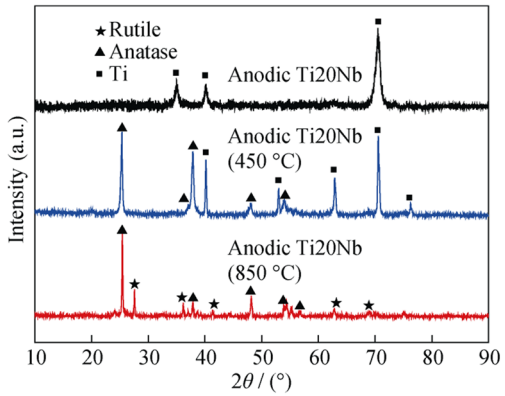

Fig. 5 XRD patterns of Ti20Nb nanotubes and Ti20Nb nanotubes after annealing at 450 and 850 °C

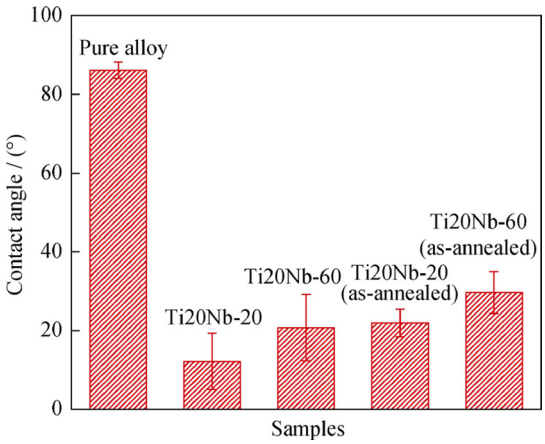

Fig. 7 Mean water contact angle of alloy, as-formed and as-annealed nanotubes anodized at 20 and 60 V

Parameters such as type of the material, surface roughness, heterogeneity of the surface, chemical composition and presence of contamination, along with the parameters related to ambient conditions, can influence surface wettability. For biological applications, the nature of hydrophobic and hydration forces plays an important role in protein adsorption and cellular adhesion. In present study, contact angle measurements were taken on intact TiNb foils and nanotubular arrays fabricated at various anodized voltages, as portrayed in Figs. 6 and 7. In order to study the effect of opening diameter of the nanotube on wettability, the nanotubular thickness of specimens fabricated by different applied voltages is maintained at about 3 μm. It is clearly shown that the nanotubular layers in all conditions are hydrophilic. The contact angles on as-formed nanotubes decrease by 70 %–80 % compared to that on the intact Ti20Nb foil. Additionally, the contact angles of the nanotube layers fabricated at 0, 20 and 60 V are found to be 86.1° ± 2.1°, 12.1° ± 7.2° and 20.7° ± 8.4°, respectively. This indicates that the hydrophilicity of the Ti20Nb nanotubes exhibits an increasing trend, since the surface becomes less hydrophilic with anodization voltage increasing from 20 to 60 V. This is likely because water easily ingresses into the smaller opening diameter tubes than the wider tubes. A similar phenomenon was observed in previous work on ZrNTs with different diameters [26]. In addition, high-temperature annealing would remove hydrogen groups, and thus, obtained annealed samples are less hydrophilic than the parent samples.

According to the Owens–Wendt (OW) method [27], the surface energy can be calculated using the following equation:

$$(1+\cos\theta)\gamma_{\mathrm{L}} = 2\left(\sqrt{\gamma_{\mathrm{L}}^{\mathrm{d}}\gamma_{\mathrm{S}}^{\mathrm{d}}} + \sqrt{\gamma_{\mathrm{L}}^{\mathrm{p}}\gamma_{\mathrm{S}}^{\mathrm{p}}}\right) \quad (1)$$

where θ is contact angle, γ_{L} denotes the liquid surface tension, $\gamma_{\mathrm{L}}^{\mathrm{d}}$ and $\gamma_{\mathrm{L}}^{\mathrm{p}}$ are its dispersive and polar components, respectively; $\gamma_{\mathrm{S}}^{\mathrm{d}}$ and $\gamma_{\mathrm{S}}^{\mathrm{p}}$ refer to the dispersive and polar

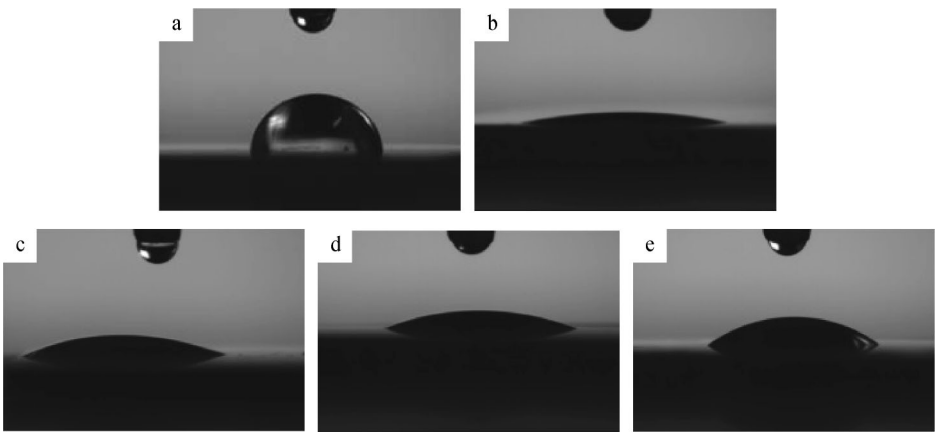

Fig. 6 Representative images of comparing contact angle measurements on Ti20Nb alloy anodized at 20 and 60 V: **a** intact, 86.1° ± 2.1°; **b** as-formed, 20 V, 12.2° ± 7.2°; **c** as-formed, 60 V, 20.8° ± 8.4°; **d** as-annealed, 20 V, 22.0° ± 3.5°; and **e** as-annealed, 60 V, 30.0° ± 5.3°

Table 2 Calculated surface energy of Ti20Nb nanotubular surfaces fabricated under various conditions ($mJ \cdot m^{-2}$)

Samples	γ_S^d	γ_s^p	γ
Pure alloy	19.1	2.7	21.8
Ti20Nb-20	20.1	51.1	71.2
Ti20Nb-60	15.6	53.0	68.6
Ti20Nb-20 (as-annealed)	16.6	51.3	67.9
Ti20Nb-60 (as-annealed)	16.0	47.8	63.8

components of the solid surface tension (γ_S), which is the sum of γ_S^d and γ_S^p. The surface tension (γ), dispersive component (γ^d) and polar component (γ^P) for water are 72.8, 21.8 and 51.0 $mJ \cdot m^{-2}$ and for glycerol are 63.4, 37.0 and 26.4 $mJ \cdot m^{-2}$, respectively [28]. Almost all of the as-formed Ti20Nb nanotubular surfaces exhibit higher surface energy. Surface energy of the as-formed Ti20Nb fabricated at different anodized voltages and the corresponding annealed Ti20Nb nanotubular surfaces, along with the alloy foil surfaces, was measured and is listed in Table 2. All as-formed Ti20Nb nanotubular surfaces exhibit higher surface energy than the intact Ti20Nb foil. By comparing the mean water contact angles of the samples, it is found that the nanotubular surfaces which are more hydrophilic exhibit higher surface energy than the intact surfaces.

Wettability of nanotubular arrays not only depends on the diameter of the tubes, but is also affected by the chemical functional groups, especially hydrophilic groups on the surface. FTIR spectroscopy was utilized to test the difference between the samples before and after annealing. As illustrated in Fig. 8, both of them portray the stretching vibration band of the hydroxyl group around 3500 cm^{-1} (Fig. 8c, d), which means that the hydroxyl group can survive even after annealing at elevated temperature. The images of hydroxyl groups (absorbance area between 3100 and 3600 cm^{-1}) in Fig. 8a, b show that the intensity of the thermally treated sample decreases to almost half of the nanotubes before thermal treatment, as the right column of the images presents the absolute value of the hydroxyl groups. Since hydroxyl groups have positive effects on wettability, decreased amount of hydroxyl groups after thermal treatment would decrease the hydrophilic properties of the sample.

In addition, the presence of fluoride ions in the samples, originating from the electrolyte during electrochemical anodization, would also have important effects on wettability. XPS was used to detect the fluoride concentration in the nanotubular arrays before and after annealing, as plotted in Fig. 9. There are considerable amounts of fluorine species present in the as-formed sample (up to 11 at%). However, after annealing treatment at 450 °C, most of the fluorine species are eliminated, as their

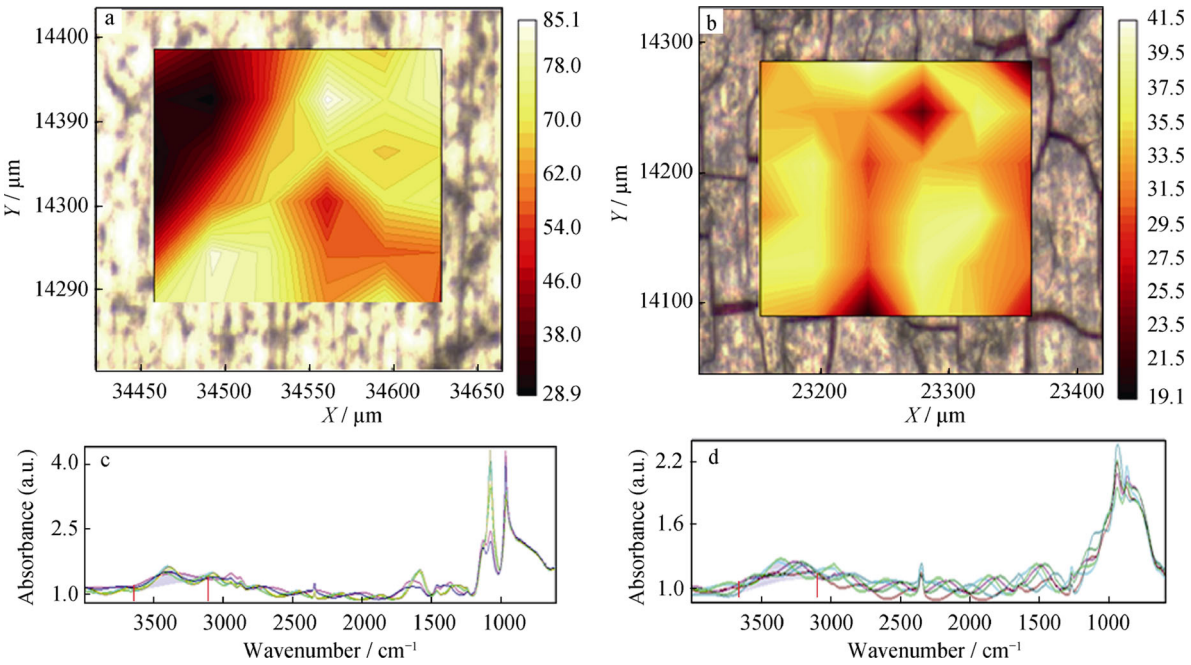

Fig. 8 FTIR spectra and corresponding typical FTIR absorption curves of Ti20Nb oxide nanotubes **a**, **c** before and **b**, **d** after thermal annealing at 450 °C (upper figures being mapping results of hydroxyl groups intensity with absorbance between 3100 and 3600 cm^{-1} in definitive region, color bars in **a** and **b** representing degree of absorbance)

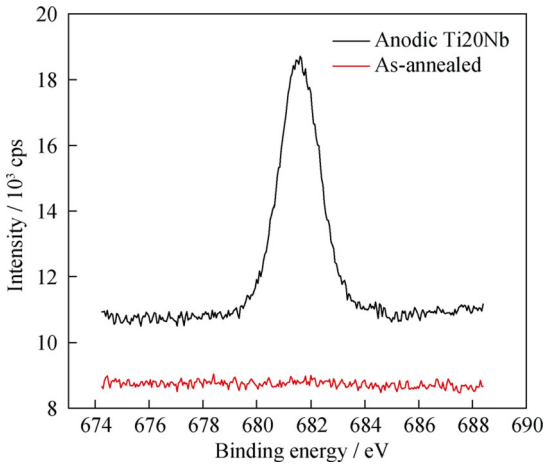

Fig. 9 XPS spectra of Ti20Nb nanotubes before and after annealing

corresponding amount decreases to less than 0.9 at%. This may be due to evaporation of HF or F_2 gas species during heat treatment, or the crystallization process trends to eject impurities out. Decreased amount of fluoride would also increase hydrophobic properties. Thus, the nanotubes after thermal annealing show higher contact angle than the samples before thermal treatment.

4 Conclusion

Anodization of Ti–*x*Nb alloys ($x = 5$ wt%–40 wt%) results in the formation of oxide nanotubular arrays with the inner diameter ranging from 40 to 50 nm, the outer diameter of approximately 120 nm and the layer thickness of approximately 10–20 μm under the studied processing conditions. Although there is a variation in geometrical factors, the Ti–*x*Nb alloy composition, particularly the Nb content, has little influence on the structure of the nanotubular arrays. The nanotubes initially form as an amorphous oxide layer on the Ti20Nb alloys. After annealing at 450 °C, XRD patterns show evidence of crystalline anatase peaks. Annealing at 850 °C results in the appearance of the rutile phase. Hydrophilic properties of the anodized nanotubular surface of Ti20Nb decrease with the applied potential, which is related to the changes in nanotube size. Water contact angle on these surfaces increases when the roughness parameters of the surface decrease. The surface energy follows the same increasing trend of the hydrophilic properties. The oxide nanotubular surfaces of Ti20Nb exhibit higher surface energy than the intact alloy. The oxide nanotubes on TiNb alloy with surface properties including hydrophilicity and roughness are more promising for biomedical applications than the intact surface of the TiNb alloys.

Acknowledgments This work was financially supported by the Beijing Higher Education Young Elite Teacher Project (No. YETP0419), the National Natural Science Foundation of China (No. 51204015), the project from Ministry of Science and Technology (No. 2014BAI11B04), and the project from the State Key Laboratory of Advanced Metals and Materials, University of Science and Technology Beijing (No. 2012Z-10).

References

[1] Lausmaa J, Kasemo B, Mattsson H, Odelius H. Multi-technique surface characterization of oxide films on electropolished and anodically oxidized titanium. Appl Surf Sci. 1990;45(3):189.
[2] Long M, Rack H. Titanium alloys in total joint replacement—a materials science perspective. Biomaterials. 1998;19(18):1621.
[3] Laing PG, Ferguson AB, Hodge ES. Tissue reaction in rabbit muscle exposed to metallic implants. J Biomed Mater Res. 1967;1(1):135.
[4] Abdel-Hady M, Hinoshita K, Morinaga M. General approach to phase stability and elastic properties of β-type Ti-alloys using electronic parameters. Scripta Mater. 2006;55(5):477.
[5] Ramarolahy A, Castany P, Prima F, Laheurte P, Péron I, Gloriant T. Microstructure and mechanical behavior of superelastic Ti–24Nb–0.5O and Ti–24Nb–0.5N biomedical alloys. J Mech Behav Biomed Mater. 2012;9(9):83.
[6] Wang Y, Dai SJ, Chen F, Yu XQ, Zhang YF. Design, strength prediction of Ti35Nb*x*Sn*y*Zr*z*Mo alloys with low elastic moduli and experimental verification on their mechanical properties. Rare Met. 2014;33(6):657.
[7] Yang YJ, Ma XM, Sun W. Design and microstructure of β-type Ti–25.6Nb–19.4Ta alloy for biomedical application. Chin J Rare Met. 2010;34(2):166.
[8] Zhuravleva K, Matthias B, Prashanth KG, Hempet U, Helth A, Gemming T, Calin M, Scudino S, Schultz L, Eckert J, Gebert A. Production of porous β-Type Ti–40Nb alloy for biomedical applications: comparison of selective laser melting and hot pressing. Materials. 2013;6(12):5700.
[9] Yao C, Webster TJ. Anodization: a promising nano-modification technique of titanium implants for orthopedic applications. J Nanosci Nanotechnol. 2006;6(9–10):2682.
[10] Grimes CA, Mor GK. TiO_2 Nanotube Arrays: Synthesis, Properties, and Applications. New York: Springer; 2009. 3.
[11] Ali G, Chen C, Yoo SH, Kum JM, Cho SO. Fabrication of complete titania nanoporous structures via electrochemical anodization of Ti. Nanoscale Res Lett. 2011;6(332):1.
[12] Gong D, Grimes CA, Varghese OK, Hu W, Singh R, Chen Z, Dickey EC. Titanium oxide nanotube arrays prepared by anodic oxidation. J Mater Res. 2001;16(12):3331.
[13] Assefpour-Dezfuly M, Vlachos C, Andrews EH. Oxide morphology and adhesive bonding on titanium surfaces. J Mater Sci. 1984;19(11):3626.
[14] Macak JM, Tsuchiya H, Ghicov A, Yasuda K, Hahn R, Bauer S, Schmuki P. TiO_2 nanotubes: self-organized electrochemical formation, properties and applications. Curr Opin Solid State Mater. 2007;11:3.
[15] Park J, Bauer S, von der Mark K, Schmuki P. Nanosize and vitality: TiO_2 nanotube diameter directs cell fate. Nano Lett. 2007;7(6):1686.
[16] von Wilmowsky C, Bauer S, Lutz R, Meisel M, Neukam FW, Toyoshima T, Schmuki P, Nkenke E, Schlegel A. In vivo evaluation of anodic TiO_2 nanotubes: an experimental study in the pig. J Biomed Mater Res B. 2009;89B(1):165.
[17] Sorkin JA, Hughes S, Soares P, Popat KC. Titania nanotube arrays as interfaces for neural prostheses. Mater Sci Eng C Mater. 2015;49(1):735.

[18] Roy P, Berger S, Schmuki P. TiO_2 nanotubes: synthesis and applications. Angew Chem Int Ed. 2011;50(13):2904.
[19] Feng XJ, Macak JM, Albu SP, Schmuki P. Electrochemical formation of self-organized anodic nanotube coating on Ti–28Zr–8Nb biomedical alloy surface. Acta Biomater. 2008;4(2):318.
[20] Jha H, Hahn R, Schmuki P. Ultrafast oxide nanotube formation on TiNb, TiZr and TiTa alloys by rapid breakdown anodization. Electrochim Acta. 2010;55(28):8883.
[21] Berger S, Faltenbacher J, Bauer S, Schmuki P. Enhanced self-ordering of anodic ZrO_2 nanotubes in inorganic and organic electrolytes using two-step anodization. Phys Status solidi (RRL) Rapid Res Lett. 2008;2(2):102.
[22] Ghicov A, Schmuki P. Self-ordering electrochemistry: a review on growth and functionality of TiO_2 nanotubes and other self-aligned MO(x) structures. Chem Commun. 2009;20(32):2791.
[23] Xu Z, Li Q, Gao S, Shang J. Synthesis and characterization of niobium-doped TiO_2 nanotube arrays by anodization of Ti–20Nb alloys. J Mater Sci Technol. 2012;28(10):865.
[24] Yasuda K, Schmuki P. Control of morphology and composition of self-organized zirconium titanate nanotubes formed in $(NH_4)_2SO_4$/NH_4F electrolytes. Electrochim Acta. 2007;52(12):4053.
[25] Gadelmawla ES, Koura MM, Maksoud TMA, Elewa IM, Soliman HH. Roughness parameters. J Mater Process Technol. 2002;123(1):133.
[26] Wang LN, Shen C, Shinbine A, Luo JL. Variation on wettability of anodic zirconium oxide nanotube surface. Thin Solid Films. 2013;531(1):277.
[27] Owens DK, Wendt R. Estimation of the surface free energy of polymers. J Appl Polym Sci. 1969;13(8):1741.
[28] Dann JR. Forces involved in the adhesive process: I. Critical surface tensions of polymeric solids as determined with polar liquids. J Colloid Interface Sci. 1970;32(2):302.